(Received 8 July 2026, Accepted 19 August 2026, Scheduled 4 September 2026)

A Dual-Port UWB MIMO Antenna with Triple Notch Characteristics Based on CPW Feeding

Jiasheng Li[1], Han Lin[1,*], Wenyan Nie[2], and Zhonggen Wang[1]

[1]School of Electrical and Information Engineering, Anhui University of Science and Technology, Huainan 232001, China
[2]School of Mechanical and Electrical Engineering, Huainan Normal University, Huainan 232001, China

ABSTRACT: This paper proposes a dual-port Ultra-Wideband (UWB) Multiple-Input Multiple-Output (MIMO) antenna with triple notch characteristics based on Coplanar Waveguide (CPW) feeding. The antenna achieves triple notch performance by introducing two L-shaped and one inverted U-shaped electromagnetic band gap (EBG) structures on the back of the substrate and etching inverted U-shaped grooves on the feed line, thereby suppressing interference from WiMAX, WLAN, and the C-band. Simulated and experimental results show good agreement, verifying the feasibility of the proposed antenna. The results show that this antenna covers the entire UWB band from 3.08 to 10.87 GHz, with a reflection coefficient of less than −10 dB, mutual coupling coefficient of less than −20 dB, envelope correlation coefficient (ECC) of less than 0.0072, and diversity gain (DG) exceeding 9.9997 dB within the operating band. It meets the requirements of high-performance MIMO systems for channel independence and transmission efficiency, and has potential applications in modern UWB communication systems.

1. INTRODUCTION

Ultra-Wideband (UWB) technology is highly valued for its high information transmission rate, wide operating bandwidth, and extremely low cost. Therefore, it is widely used in 5G communication, short-range communication, positioning, tracking, and radar fields [1, 2]. Common methods for extending the bandwidth of traditional microstrip antennas include: thickening the dielectric substrate, using a multilayer structure, changing the radiating patch, and employing loading techniques. Among them, changing the radiating patch is the most common and practical method, as it alters the antenna's radiation performance and characteristic impedance by changing the patch's shape. However, UWB antennas may be subject to interference from various commonly used communication frequency bands, such as WiMAX, WLAN, and X-band used by satellite communication [3]. To ensure the reliable operation of existing wireless communication systems, it is crucial to suppress interference of these frequency bands on UWB antennas. UWB antennas with notch characteristics designed for this purpose are a mainstream solution in the industry [4]. A notch is a band that introduces a stopband in a specific frequency range to impede signal transmission. This stopband is called the notch band. Currently, traditional techniques for achieving notch characteristics include adding parasitic elements to the radiating element, feed line, or ground plane [5], electromagnetic bandgap (EBG) [6], or etching different types of grooves on the radiating patch or ground plane [7]. Coplanar waveguide feeding is a commonly used feeding method for UWB antennas. A traditional notch generation structure on UWB antennas fed by coplanar waveguides (CPW) is on the front side of the substrate, but the back side is not effectively utilized. For example, in [8], two notches were generated in the WIMAX band (3.3–3.7 GHz) and the military/radar band (8.2–8.6 GHz) by etching H-shaped and symmetrical U-shaped slots on the radiating patch, respectively. In [9], dual-notch characteristics were achieved in the WIMAX band (3.1–3.9 GHz) and WLAN band (5.1–5.6 GHz) by etching symmetrical S-shaped slots on ground planes on both sides and etching circular slots on the radiating patch, respectively. It can be seen that most notch structures are concentrated on the radiating patch or the ground plane. At the same time, traditional UWB technology still faces the challenge of multipath effects. To solve this problem, the industry has proposed Multiple-Input Multiple-Output (MIMO) technology [10]. However, coupling between ports seriously affects the performance of MIMO antennas. Therefore, various decoupling measures are usually used to enhance port isolation, thereby reducing the impact of inter-unit coupling on antenna performance [11]. MIMO decoupling technology achieves optimization via three aspects: innovative antenna structure design to reconstruct the electromagnetic field distribution at the physical level, introducing decoupling networks to establish reverse coupling channels and achieve phase cancellation, and applying advanced signal-processing algorithms to perform coupling compensation in the digital domain. For example, physical isolation [12], defective ground structures [13], neutralization lines [14], and other methods are used to weaken the mutual coupling effect [15]. Functions of UWB, MIMO technologies are fully used in UWB MIMO antennas, further improving channel capacity and communication rate, and reducing the impact of multipath fading [16], making them highly suitable for advanced scenarios, including self-diplexing designs for biomedical applications [17–19].

* Corresponding author: Han Lin (hanlin@aust.edu.cn).

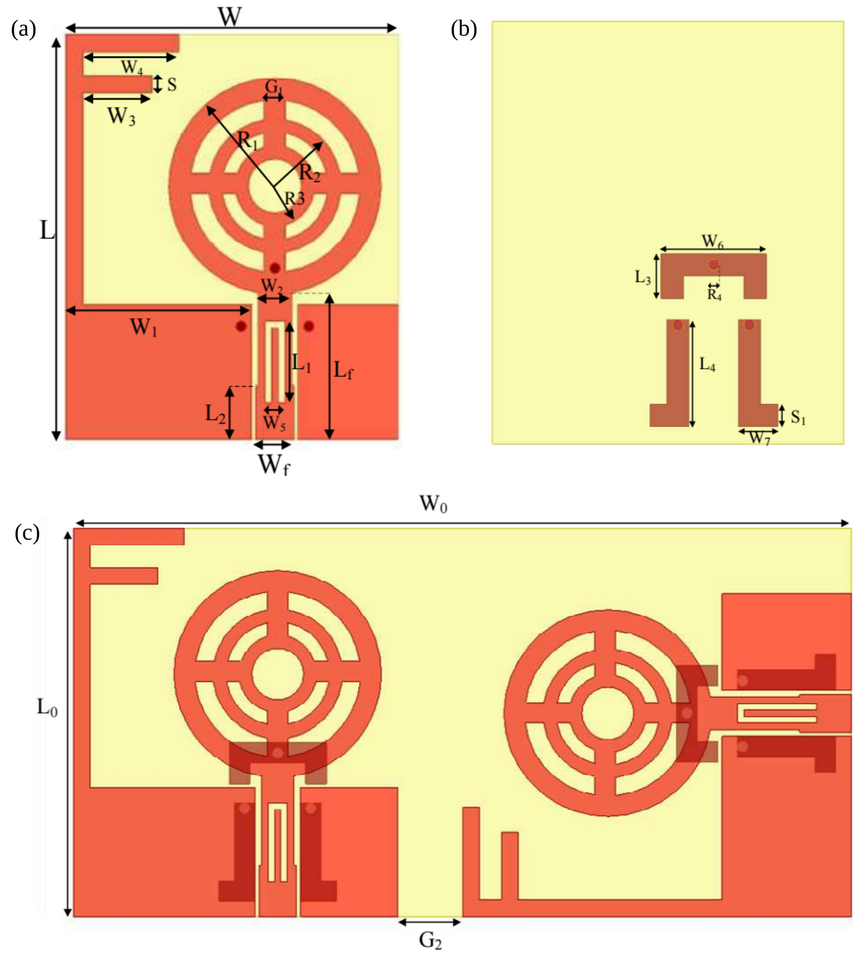

FIGURE 1. Geometry of the proposed UWB MIMO antenna: (a) top view, (b) bottom view, and (c) total view.

To address the underutilization of the backside of CPW-fed antennas, this paper proposes a UWB MIMO antenna with triple-notch characteristics based on CPW feeding. By combining L- and inverted U-shaped EBG structures on the back of the substrate with inverted U-shaped slots on the feed line, this antenna successfully achieves precise notch suppression across three different frequency bands: WiMAX, WLAN, and C-band. Both simulated and experimental results demonstrate that this antenna has excellent impedance matching performance, low mutual coupling, good diversity performance, and notch characteristics across the entire UWB frequency, providing a feasible solution for various portable wireless applications. The core contributions and key technical innovations of this work can be summarized as follows:

(1) Unlike traditional UWB MIMO antennas that concentrate the notch structure on the front side of the substrate, this method (combining the EBG structure on the back side of the substrate with feed slots) ensures that the notch is independent of the patch and ground plane, which is the main difference between it and previous UWB MIMO antennas. This design can achieve notch effects in the 3.9 GHz, 5.8 GHz, and 7.4 GHz bands while maintaining good impedance matching.

(2) This design moves the notch structure of a traditional CPW-fed antenna to the back of the substrate, allowing notch structures to be loaded on both the front and back of the substrate simultaneously, thus generating more notch bands on the same substrate. It improves the antenna's space utilization while maintaining the independence and integrity of each notch structure.

2. ANTENNA DESIGN PROCESS

2.1. Antenna Geometry

Fig. 1 show the antenna geometry. The antenna was printed on an FR4 dielectric substrate with a relative permittivity of 4.4, loss tangent of 0.02, and overall dimensions of 60 mm $\times$ 30 mm $\times$ 1.6 mm. This paper uses ANSYS HFSS 21 software for simulation. As shown in Fig. 1(a), the substrate's front side uses a CPW feed, extending the current path through an improved circular radiating patch and an F-shaped stub on the left ground plane to achieve UWB characteristics. An inverted U-shaped groove is also etched on the feed line to create a notch. As shown in Fig. 1(b), the substrate's back side uses EBG unit structures, with an inverted U-shaped patch at the center and two L-shaped patches below it. This structure consists of patches and short-circuit vias located at the center and end of the patches, thus generating two notches. Fig. 1(c) shows

TABLE 1. Antenna parameter dimensions.

Parameters	L_0	L_1	L_2	L_3	L_4	W_0	W_1
Value (mm)	30	6	4	3.2	7.6	60	14
Parameters	W_2	W_3	W_4	W_5	W_6	W_7	R_1
Value (mm)	2.5	5.2	7.2	1.5	7.5	2.8	8
Parameters	R_2	R_3	R_4	S	S_1	G	G_1
Value (mm)	4.8	4	1.6	1.3	1.6	0.3	1.6

the final UWB MIMO antenna, and Table 1 summarizes final optimized dimensional parameters.

Figure 2 shows that the antenna achieves good impedance matching in the 3.08–10.87 GHz frequency band. Furthermore, it forms distinct notch bands in the 3.30–4.31 GHz, 4.82–6.32 GHz, and 6.60–7.71 GHz frequency bands. Throughout the operating frequency band, the antenna exhibits good isolation performance, with a coupling coefficient S_{12} lower than -20 dB.

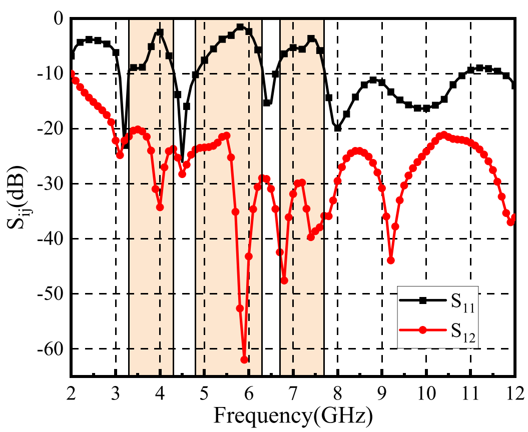

FIGURE 2. Simulated S-parameters of the proposed triple-notched MIMO antenna characteristics.

2.2. UWB Antenna Evolution

Fig. 3 shows the UWB antenna design process, and Fig. 4 shows S_{11} curves for each stage. To clearly describe the antenna evolution, the antennas at each stage were labeled as Ant1 to Ant3. The characteristic impedance of the CPW feed used in this paper is 50 ohms, which can be calculated using formulas (1) to (4):

$$Z_0 = \frac{30\pi K'(k_1)}{\sqrt{\varepsilon_{eff}}K(k_1)} \tag{1}$$

$$\varepsilon_{eff} = 1 + \frac{\varepsilon_r - 1}{2} \times \frac{K(k_2)K'(k_1)}{K'(k_2)K(k_1)} \tag{2}$$

$$k_1 = \frac{W_f}{W_f + 2s}\sqrt{\frac{1-(W_f+2s)^2}{W^2}1 - \frac{W_f^2}{W^2}} \tag{3}$$

$$k_2 = \frac{\sinh(\pi W/4h)}{\sinh(\pi(W_f+2S)/4h)} \times \sqrt{\frac{1-\sinh^2(\pi(W_f+2S)/4h)/\sinh^2(\pi W/4h)}{1-\sinh^2(\pi W_f/4h)/\sinh^2(\pi W/4h)}} \tag{4}$$

where h, W, W_f, S, ε_r, and ε_{eff} are the height and width of the dielectric substrate, the width of the CPW feed line, the distance between the feed line and the ground plane, and the relative permittivity and effective permittivity of the dielectric substrate, respectively, and $K(k)$ and $K'(k)$ represent the first-order elliptic complete integral function and the supplementary function, respectively.

The above formula shows the relationship between the characteristic impedance of the CPW feed and various parameters. With a dielectric substrate width of 20 mm, only the feed line width w and spacing s are undetermined. Therefore, when the feed line width is 2.8 mm, the gap between the feed line and the ground plane is 0.3 mm.

Ant1 comprises a circular radiating patch and rectangular ground planes on both sides. The antenna's radiating patch is circular. The circular edge is smoother, and the surface current distribution is relatively uniform. It does not cause surface current accumulation due to abrupt changes in the edge structure. The simulation results show that its operating frequency range is only 3.1–4.6 GHz, which means that the impedance-matching effect is poor in most target frequency bands, far from meeting the bandwidth requirements of UWB antennas. To improve the impedance matching characteristics across the entire frequency band, an F-shaped stub was added to the left ground plane of Ant1. This structure effectively extended the current path and introduced a resonant point at 6 GHz, improving the antenna's impedance-matching characteristics. The bandwidth of Ant2 extends to 3.5–4.41 GHz, 5.71–6.07 GHz, and 7.05–9.43 GHz. To further extend the bandwidth, Ant3 adopts an improved circular radiating patch and stepped feed structure. An improved circular radiating patch was created by introducing annular slots in the original circular radiating patch. This improved patch extends the current path and enhances resonance capability, thus improving the antenna's impedance matching. Furthermore, the upper part of the rectangular microstrip line was adjusted to form a stepped feed structure, effectively lowering the cutoff frequency in the low-frequency band. The combined effect of these two factors results in a new resonant point and a wider bandwidth for the antenna. Its final operating frequency band is 3.3–12 GHz, meeting requirements of a UWB antenna.

Figures 5(a) and (b) show Ant2's current distribution at 7.8 GHz and Ant3 at 8.3 GHz, respectively, to illustrate the contribution of the resonant mode excitation of the center patch to the overall impedance bandwidth. Ant3's structural improvements fundamentally change the current flow; introducing an annular groove forces the current to propagate along the edges of these new structures, effectively extending the current path across the entire patch surface. Therefore, it shifts the high-frequency resonant point from 7.8 GHz to 8.3 GHz, improves impedance matching in the high-frequency band, and helps to broaden the UWB's operating bandwidth.

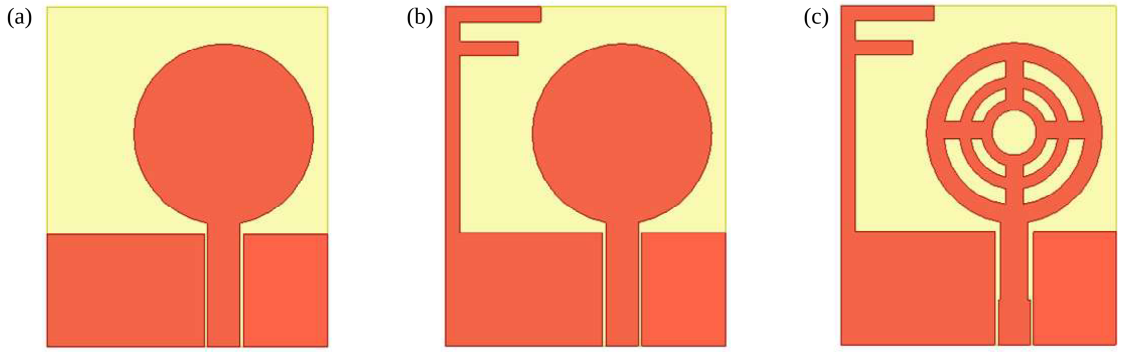

FIGURE 3. The UWB antenna evolution: (a) Ant 1, (b) Ant 2, and (c) Ant 3.

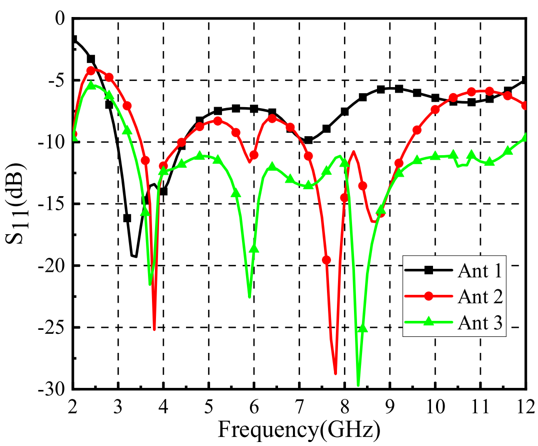

FIGURE 4. Parameters of the monopole UWB antenna.

2.3. Notch Antenna Evolution

To suppress narrowband interference in the UWB, a multi-band notch filter structure is designed. Fig. 6 shows the specific evolution process, and Fig. 7 shows the corresponding S_{11} curves. First, based on Ant3, two symmetrical L-shaped EBG structures were added to the back of the substrate. This structure connects the patch to the ground plane through vias in the substrate, forming a notch filter band of 3.3–4.31 GHz(center frequency 3.9 GHz). Based on Ant4 design, an inverted U-shaped EBG structure was added to the back of the improved circular radiating patch in the same manner, successfully forming a notch filter band of 4.82–6.32 GHz (center frequency 5.8 GHz). Finally, an inverted U-shaped groove was etched on Ant5's feed line, forming a notch filter band of 6.60–7.71 GHz (center frequency 7.4 GHz). With the above design, the proposed antenna achieves three-band notch filter performance. This system can suppress interference from narrowband communication systems, including WiMAX, WLAN, and C-band, while maintaining coverage of the UWB operating frequency band from 3.2–12 GHz.

Figure 8 shows the antenna's current vector distribution at different notch-center frequencies. The current direction of the patch intuitively reveals the design principle of notch characteristics. Fig. 8(a) shows that at 3.9 GHz, the current is mainly concentrated on ground planes on both sides of the feed line and corresponding L-shaped patches below them. At this time, the vector current flows along the upper and lower sides of the cylindrical aperture, forming a mutually repulsive current field in this region. This interaction of current fields effectively suppresses antenna radiation capability, resulting in a significant notch band at approximately 3.9 GHz. Fig. 8(b) shows that at 5.8 GHz, similar to the formation of the first notch, the current concentrates flowing through the copper pillars on the inverted U-shaped patch, and then diffuses from the copper pillars to the inverted U-shaped slot. This process forms a reverse electric field, hindering the antenna's radiation effect, and ultimately leading to a notch band at 5.8 GHz. Fig. 8(c) shows that at 7.4 GHz, the current is mainly concentrated near the inverted-U-shaped slot. After the current enters the feeder, most of it propagates along both sides of the inverted U-shaped slot and eventually converges at the gap between the two slots, forming a locally circulating current. This circulating current confines the current to the two arms of the inverted U-shaped structure, resulting in almost no effective radiation near the 7.4 GHz band, thus forming a notch band at 7.4 GHz.

2.4. Dual-Port MIMO Antenna Evolution

To improve the overall antenna signal performance and data transmission efficiency, this section discusses the design scheme and isolation performance of a two-port MIMO antenna. Placing two antennas orthogonally enables the radiation of orthogonally polarized waves or forming complementary radiation patterns. It naturally leads to low correlation in their far-field signals in multipath-rich environments, thus achieving decoupling. Figs. 9(a)–(d) show four different arrangement schemes designed to determine the optimal position of the MIMO antenna. Fig. 10 shows the antenna's S_{11} and S_{12} curves at various positions. From the S_{12} curve in Fig. 10(a), it can be seen that the isolation was at position.1, below -20 dB throughout the operating frequency band, whereas the isolation at position.3 is only below -10 dB. Although the isolation at positions.2 and 4 is mostly below -20 dB, the S_{11} curve in Fig. 10(b) shows that position.1 has better impedance-matching characteristics and notch-filtering performance within the same frequency band. In summary, position.1 has superior notch-filtering performance and better isolation characteristics; therefore, Fig. 9(a) was selected as the arrangement scheme for this two-port MIMO antenna.

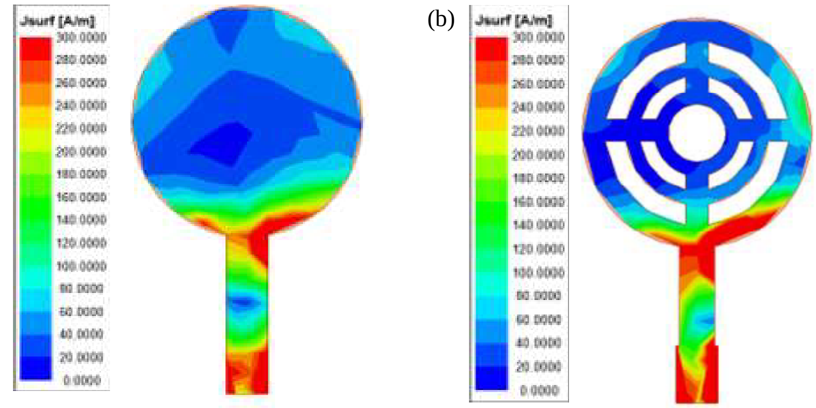

FIGURE 5. Surface current of the central patch, (a) Ant 2 at 7.8 GHz and (b) Ant 3 at 8.3 GHz.

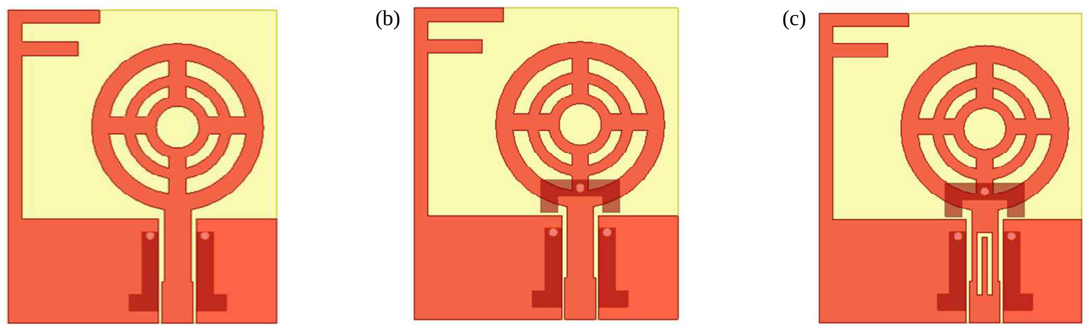

FIGURE 6. Band-notch antenna evolution process: (a) Ant 4, (b) Ant 5, and (c) Ant 6.

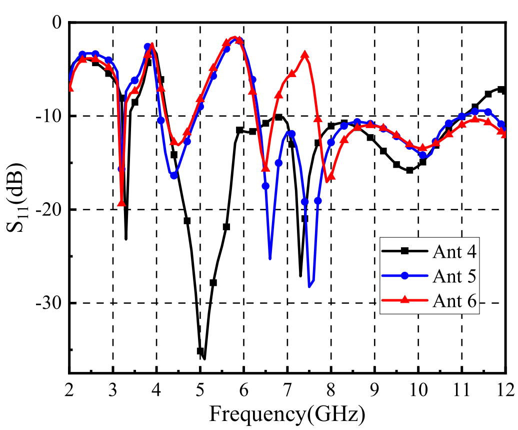

FIGURE 7. Parameters of the band-notch antenna.

Figure 11 shows the current distribution of the MIMO antenna in Fig. 9(a) at 3.2 GHz, 4.5 GHz, 6.5 GHz, and 8.0 GHz. The overall antenna dimensions are 60 mm × 30 mm × 1.6 mm; the operating frequency range is 3.08–10.87 GHz; and the port isolation exceeds -20 dB. As can be seen in Figs. 11(a)–(d), the current at different frequencies is mainly concentrated in and around the feed line of the left antenna, whereas only a weak current is generated in the right antenna. This indicates that an orthogonal placement structure can reduce coupling between antennas, and this method can improve isolation without adding an isolation structure to the antenna. In summary, this scheme enhances port isolation, thereby improving the overall performance of the MIMO antenna.

Figure 12 shows the influence of various structural parameters on antenna S-parameters. As can be seen from Fig. 12(a), the antenna's impedance matching deteriorates as feed line width increases, while the notch bandwidth does not change significantly. Fig. 12(b) shows that floor height has a significant impact on the antenna's impedance matching and notch bandwidth. When the floor height is too large, the antenna's matching performance in the mid-frequency band deteriorates severely. In summary, a value of 2.9 mm for W_f and 10 mm for L_0 are the optimal choice.

3. ANTENNA PERFORMANCE ANALYSIS

3.1. Antenna S-Parameter Analysis

Simulation data of the antenna shown in Fig. 13(a) were experimentally verified using an N5230A vector network analyzer. The radiation patterns were measured in an anechoic chamber using a standard-gain horn antenna, with the measurement setup shown in Fig. 13(b). Figs. 14(a) and (b) show S_{11} and S_{12} parameters in the simulation and measurement, respectively.

Figure 14(a) shows that the measured and simulated S_{11} values are in good agreement. There are slight differences between the measured reflection coefficient curve and the actual measurement. The first two notch curves have lower notch depths and wider notch bandwidths. The measured results of

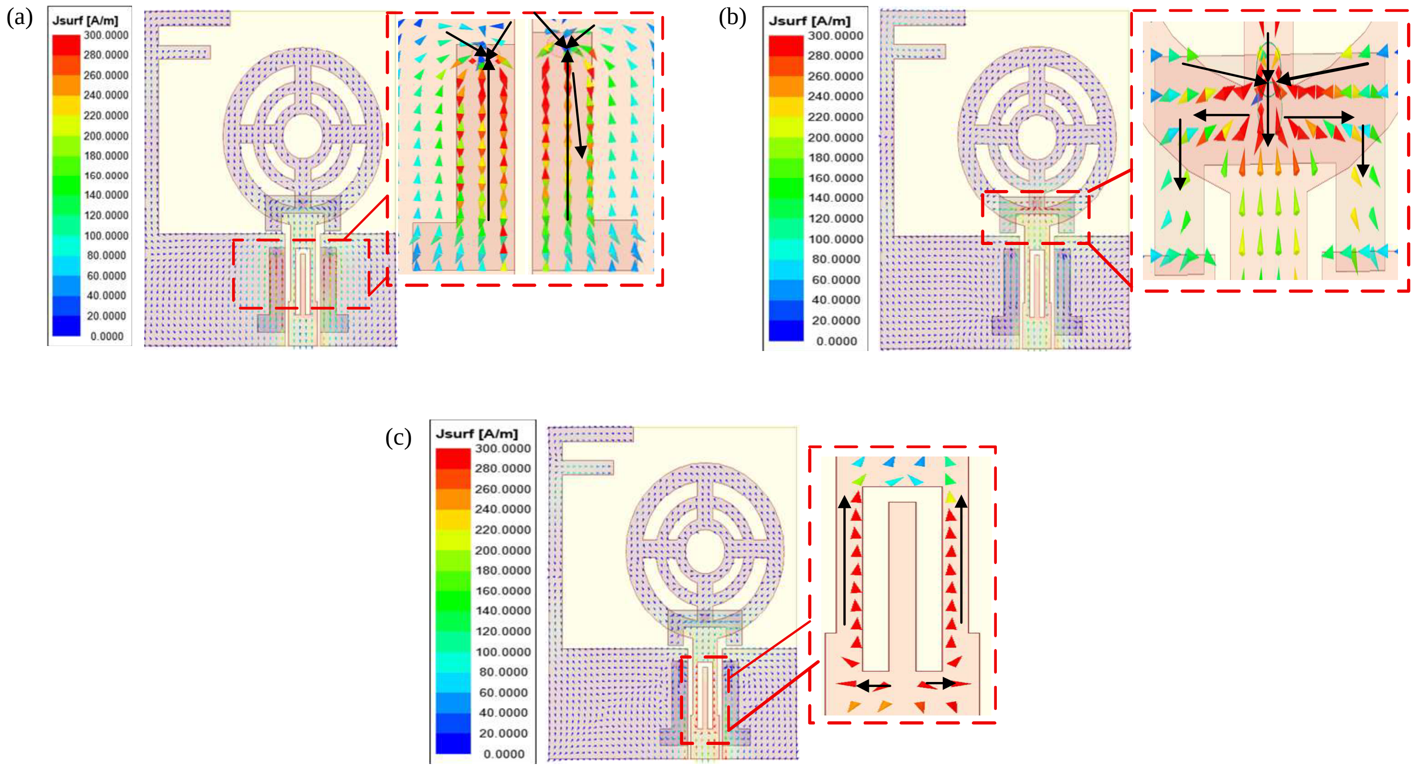

FIGURE 8. Vector current diagram, (a) 3.9 GHz, (b) 5.8 GHz, and (c) 7.4 GHz.

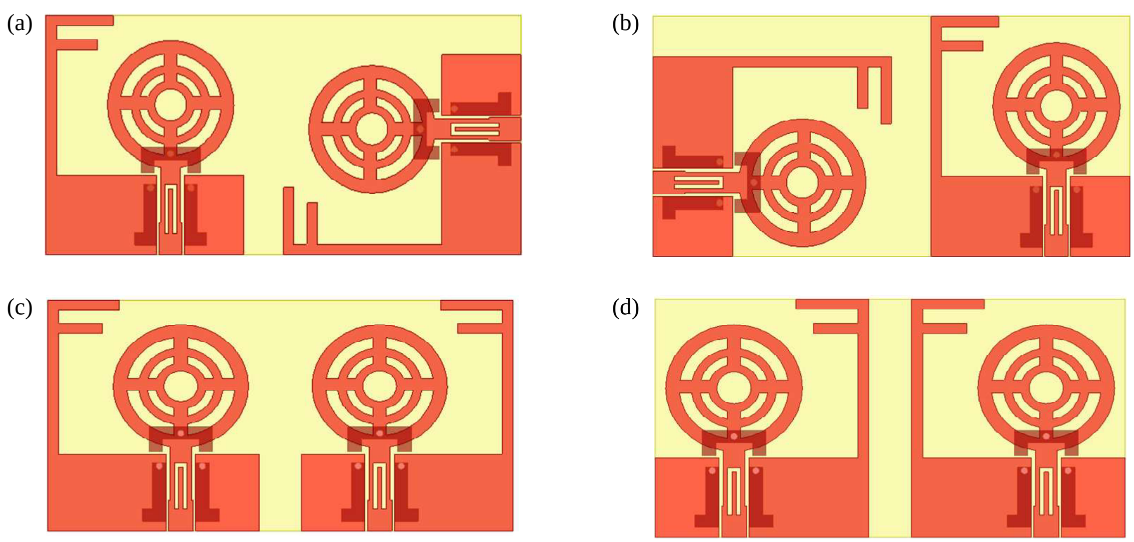

FIGURE 9. Various positioning for MIMO antenna development: (a) Position 1, (b) Position 2, (c) Position 3, and (d) Position 4.

the third notch curve are basically consistent with the simulation results. The measured antenna has a relative bandwidth of 96.3% in the range of 3.71–10.6 GHz and exhibits triple-notch characteristics at 4 GHz, 6.2 GHz, and 7.4 GHz. It can be observed that there is a certain error between the measured and simulated values. The small difference between measured and simulated values arises from the SMA connector loss and manufacturing tolerance. Fig. 14(b) shows the antenna's isolation performance, in which the measured antenna isolation differs from simulated one because the testing environment alters the coupling between MIMO antenna elements. Measured and simulated antenna mutual coupling coefficients exceed −20 dB throughout the entire operating frequency band, fully verifying the antenna's excellent port isolation performance.

3.2. Envelope Correlation Coefficient and Diversity Gain

The performance of the proposed MIMO antenna was evaluated using the envelope correlation coefficient (ECC) and diversity gain (DG). Theoretically, a completely uncorrelated di-

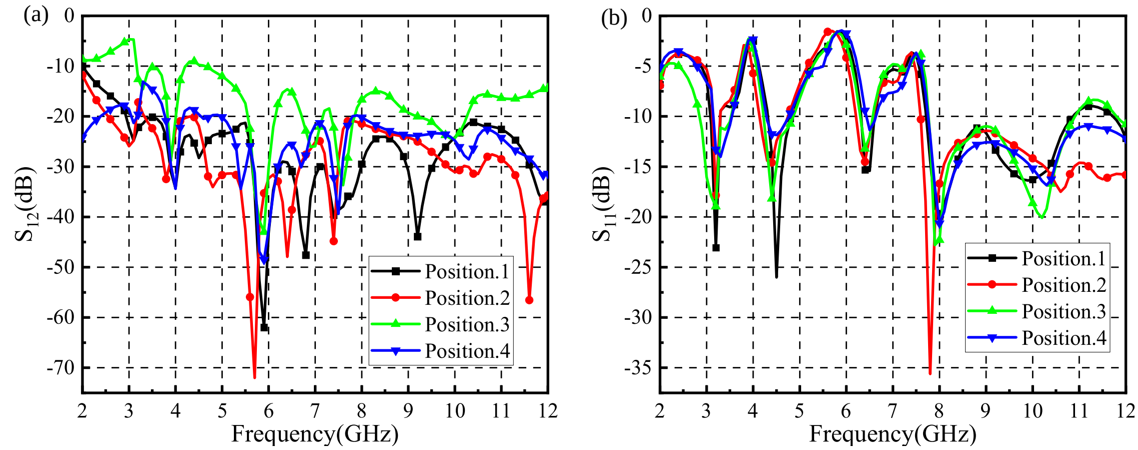

FIGURE 10. Simulated isolation characteristics and S-parameters of the two-port MIMO for various positions: (a) S_{11} and (b) S_{12}.

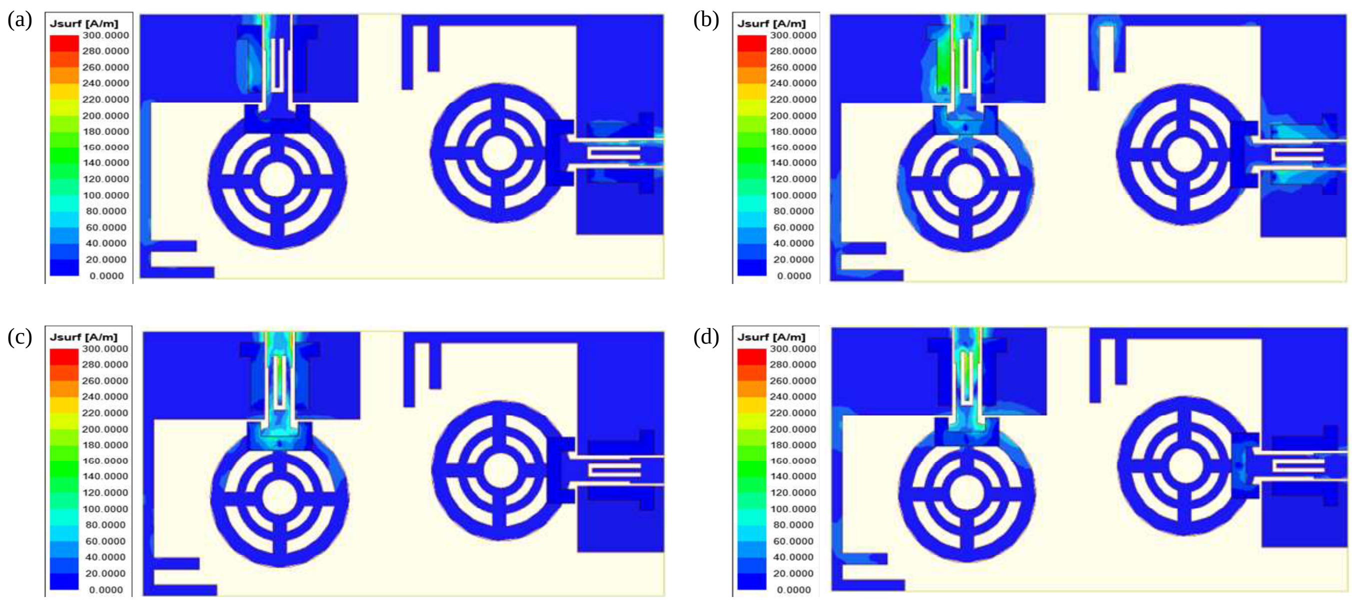

FIGURE 11. Current distribution diagram at (a) 3.2 GHz, (b) 4.5 GHz, (c) 6.5 GHz, and (d) 8.0 GHz.

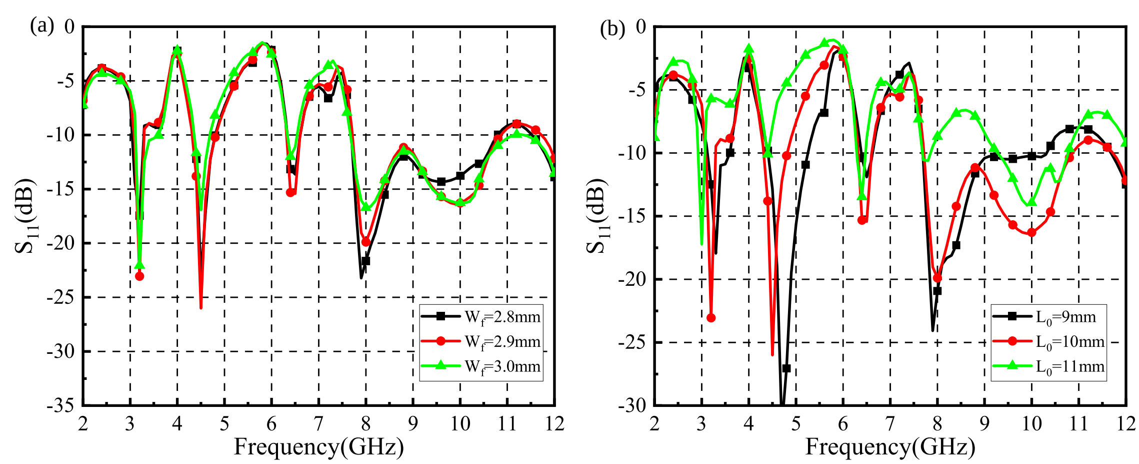

FIGURE 12. Influence of various structural parameters on antenna S-parameters: (a) feeder width W_f and (b) floor height L_0.

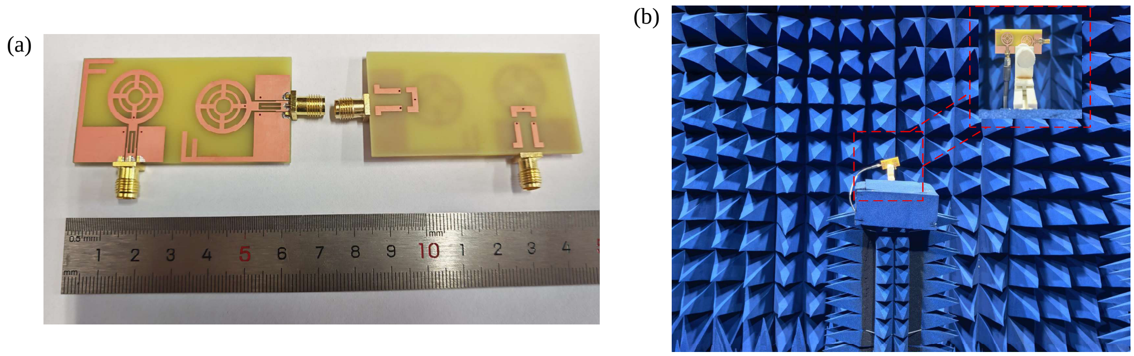

FIGURE 13. (a) The proposed antenna fabricated prototype and (b) measured results in a microwave anechoic chamber.

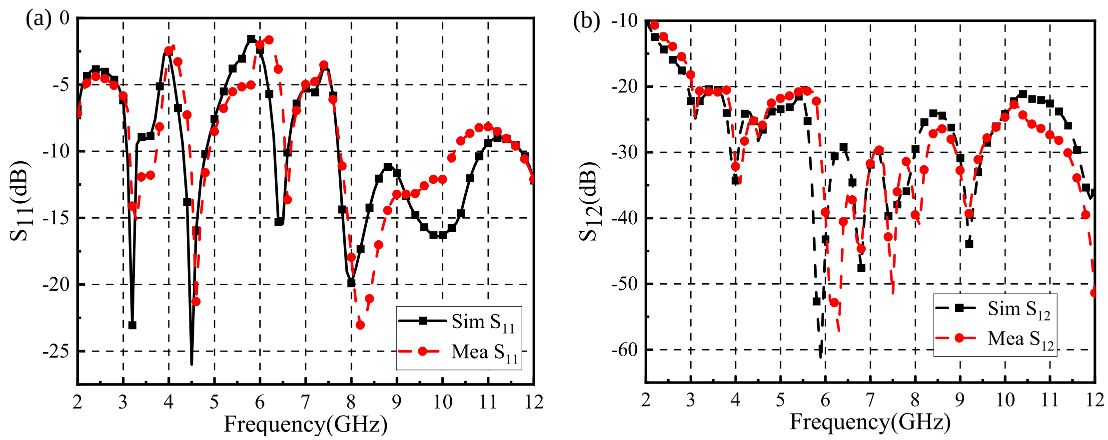

FIGURE 14. Simulated and measured S-parameters of the proposed antenna: (a) S_{11} and (b) S_{12}.

versity antenna should have an ECC value of zero; however, in practical applications, the general standard requires an ECC value of lower than 0.5. When the ECC value of the MIMO system is significantly reduced, it ensures that each spatial data stream undergoes independent fading. Ideally, a near-zero ECC value indicates that the channel has high orthogonality, meaning that each antenna operates in a different scattering environment without significant interference. This decoupling phenomenon is a fundamental prerequisite for fully using the potential of spatial multiplexing and diversity gains. Therefore, antenna arrays with good decoupling characteristics can directly improve the overall channel capacity, enhance link reliability, and effectively suppress mutual interference. The formula for calculation using radiation parameters is as follows:

$$\rho_e = \frac{\left|\iint 4\pi \left[F_i(\theta,\phi) * F_j(\theta,\phi)\right] d\Omega\right|^2}{\iint 4\pi \left|F_i(\theta,\phi)\right|^2 d\Omega \iint 4\pi \left|F_j(\theta,\phi)\right|^2 d\Omega} \quad (5)$$

DG is a macroscopic theoretical metric that measures the system resistance to signal attenuation. It represents a significant reduction in the fading margin or signal-to-noise ratio (SNR) required for a given reference outage probability when employing diversity combining techniques (such as maximum ratio combining in multipath fading channels). In an ideal MIMO system composed of completely uncorrelated antenna elements, the maximum theoretical diversity gain achievable in a Rayleigh fading environment is 10 dB. As the inter-antenna correlation increases, the achievable diversity gain decreases accordingly, directly affecting the reliability of the communication link. Theoretically, effective diversity gain is inversely proportional to the system's envelope correlation. DG can be calculated using ECC, and the formula for calculating DG is as follows:

$$DG = \sqrt{1 - ECC^2} \quad (6)$$

As shown in Fig. 15, ECC and DG performance indicators using S-parameters are less than 0.0072 dB and greater than

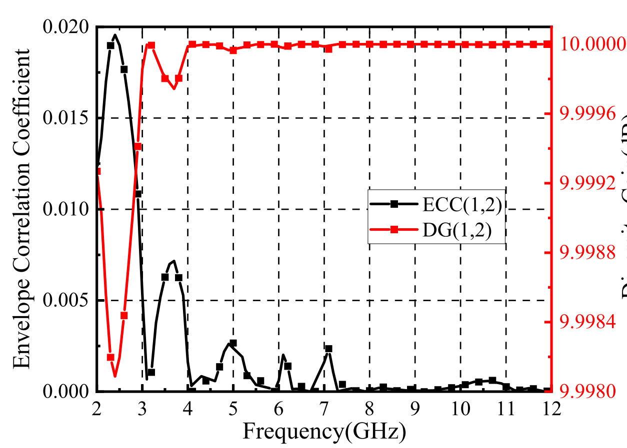

FIGURE 15. ECC and DG.

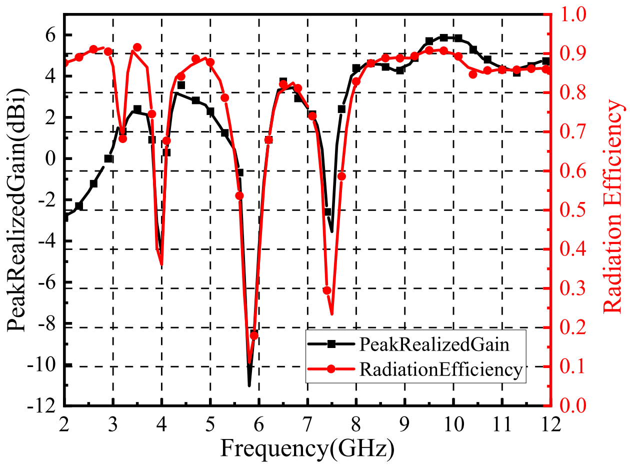

FIGURE 16. Antenna peak realized gain and radiation efficiency.

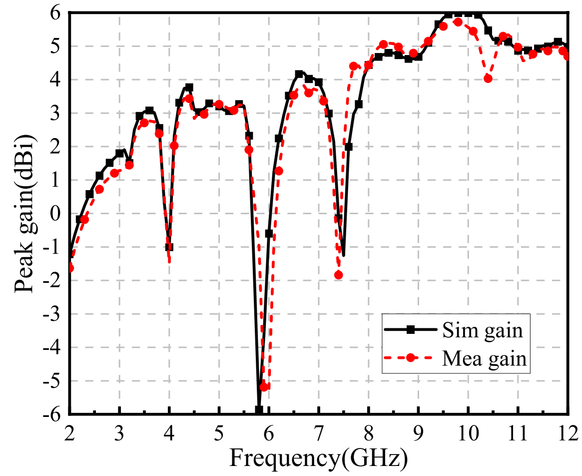

FIGURE 17. Simulated and measured Peak gain.

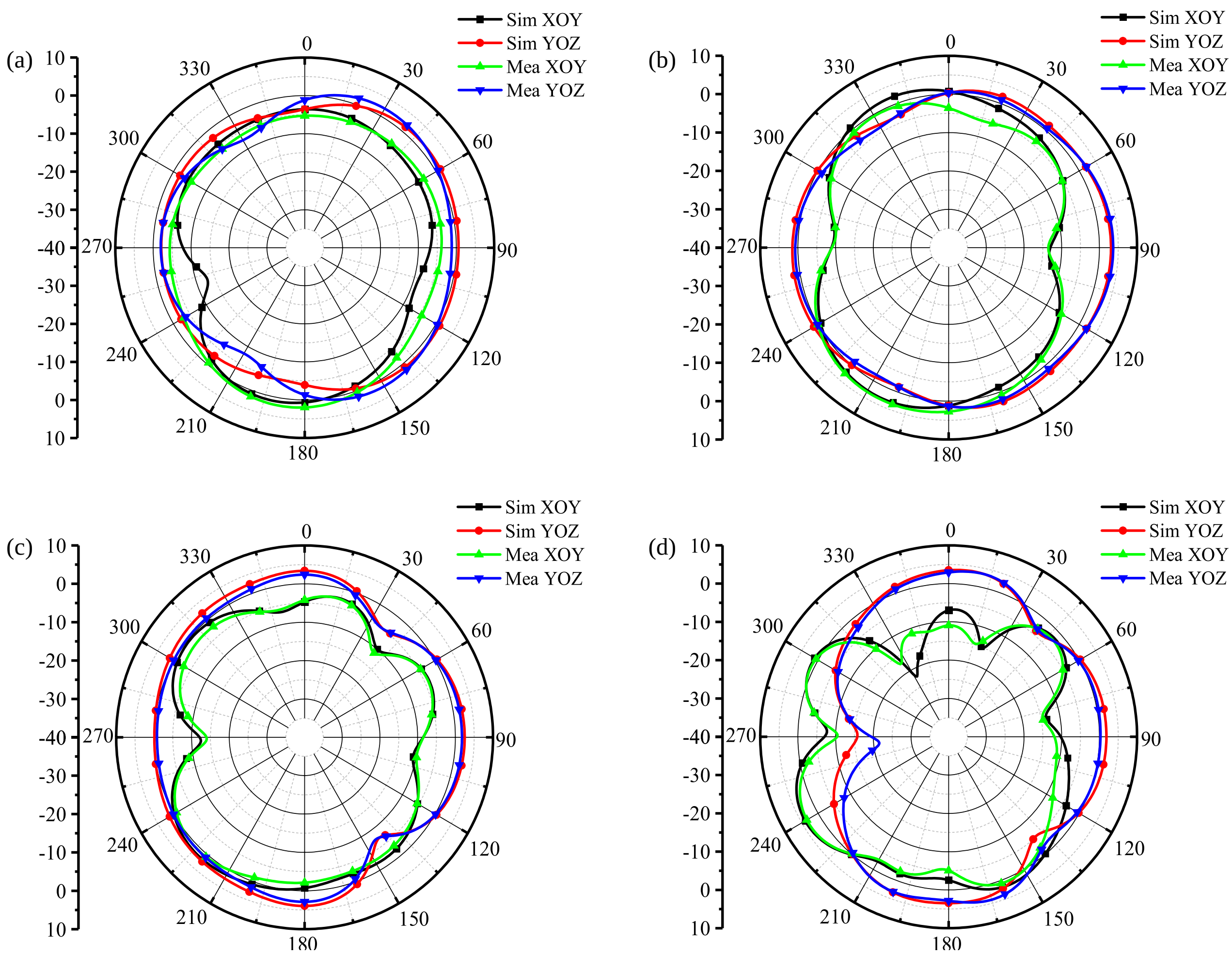

FIGURE 18. 2D radiation patterns at (a) 3.2 GHz, (b) 4.5 GHz, (c) 6.5 GHz, and (d) 8.0 GHz.

9.9997 dB, respectively. The simulation results show that this antenna element achieves ultra-low correlation and excellent diversity characteristics, effectively avoiding mutual interference during operation and significantly improving the signal transmission efficiency.

3.3. Antenna Gain and Efficiency Analysis

Figure 16 shows the antenna's simulated efficiency and peak realized gain, and Fig. 17 illustrates port 1's measured and simulated peak gains. Port 2's gain is almost identical to port 1's. As shown in Fig. 16 and Fig. 17, the antenna maintains a high

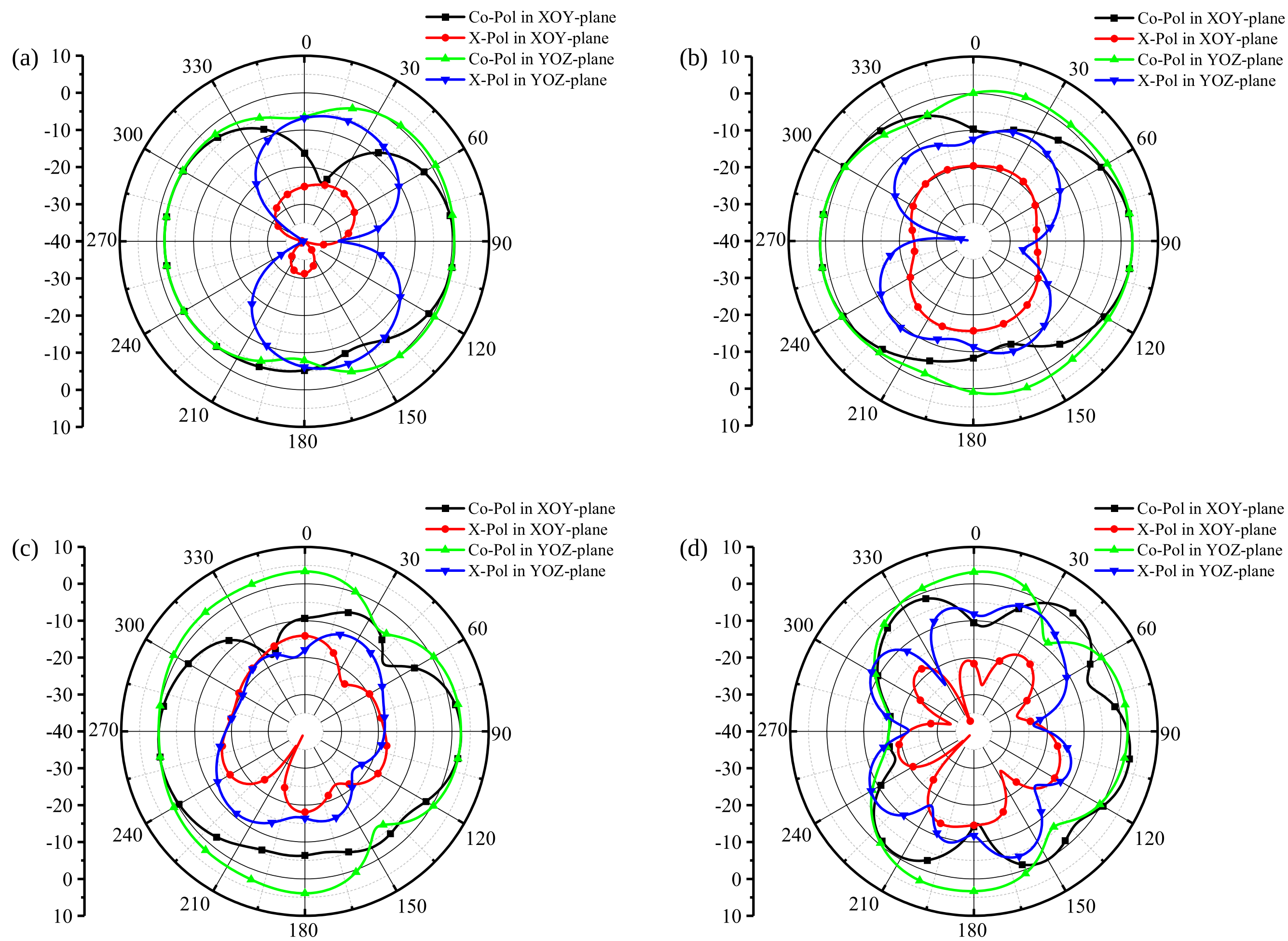

FIGURE 19. Co- and cross-polarization modes at (a) 3.2 GHz, (b) 4.5 GHz, (c) 6.5 GHz, and (d) 8.0 GHz.

radiation efficiency (over 80%) outside the notch band, and its actual peak gain fluctuated stably between 2 dBi and -6 dBi across the entire UWB. The gains at the center frequencies of each notch band were -4.6 dBi, -11 dBi, and -3.5 dBi, corresponding to radiation efficiencies of 36%, 11%, and 23%, respectively. This indicates that signals within the notch frequency range can be effectively suppressed, further demonstrating stable signal suppression performance within the notch frequency range. Furthermore, the antenna maintained a high gain and efficiency outside the notch region, indicating that the antenna's notch structure did not significantly affect overall radiation characteristics in the UWB operating band.

3.4. Antenna Radiation Performance Analysis

Figure 18 illustrates two-dimensional radiation modes of the proposed UWB MIMO antenna at four resonant points (3.2 GHz, 4.5 GHz, 6.5 GHz, and 8.0 GHz). The results show that at 3.2 GHz and 4.5 GHz, the antenna exhibits excellent omnidirectional radiation characteristics in the H-plane and forms a good bidirectional radiation mode in the E-plane. As the operating frequency increases to 6.5 GHz and 8.0 GHz, the radiation mode begins to show some distortion, but the antenna still maintains good omnidirectional radiation performance at higher frequencies. Furthermore, the simulation results at the test frequencies were in good agreement with the measured data, verifying the design's rationality. Overall, this dual-port MIMO antenna maintained stable radiation characteristics throughout the entire operating frequency band, meeting practical application requirements of broadband communication.

Figure 19 illustrates co-polarization (Co-Pol) and cross-polarization (X-Pol) components in the XOY and YOZ planes. As shown, in the low-frequency bands of 3.2 GHz and 4.5 GHz, co-polarization consistently dominates, while cross-polarization is significantly suppressed in almost all observation directions, exhibiting excellent polarization purity. As the frequency increases to 6.5 GHz and 8.0 GHz, slight distortion and fluctuations appear in co-polarization, but cross-polarization remains effectively controlled, well below the co-polarization peak. Maintaining low cross-polarization throughout the entire measurement band confirms that the proposed antenna can effectively reduce polarization mismatch loss, ensuring reliable, high-quality signal transmission in practical UWB environments.

Figure 20 shows three-dimensional radiation patterns of the proposed UWB MIMO antenna at corresponding resonant frequencies (3.2 GHz, 4.5 GHz, 6.5 GHz, and 8.0 GHz). As

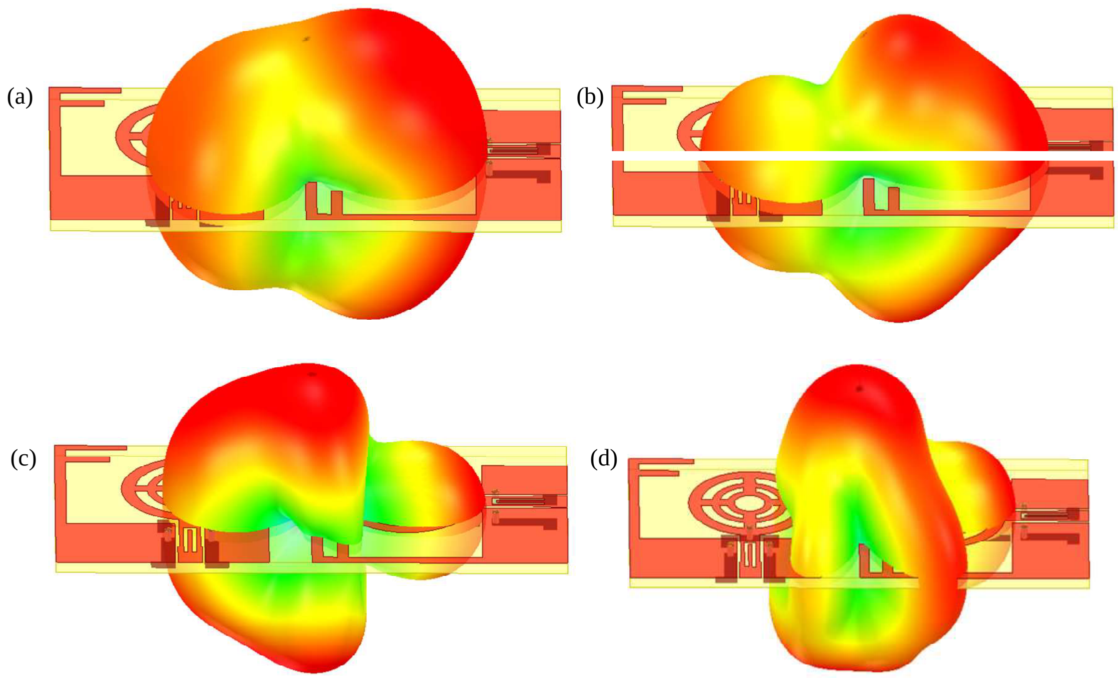

FIGURE 20. 3D radiation patterns at (a) 3.2 GHz, (b) 4.5 GHz, (c) 6.5 GHz, and (d) 8.0 GHz.

TABLE 2. Comparison of the proposed antenna with several existing antennas.

Ref.	Size (mm^2)	BW (GHz)	No. of notches	No. of ports	Isolation (dB)	ECC	Year
[20]	44×39	3.3–9.9	/	/	/	/	2019
[21]	18×36	3–11	2	2	< -20	< 0.05	2020
[22]	30×30	2.5–10.8	2	2	< -20	< 0.004	2022
[23]	21.5×28	3.1–10.6	2	2	< -16	< 0.3	2022
[24]	35.9×35.9	3.2–10.8	3	4	< -19	< 0.49	2023
[25]	90×70	5.1–7	/	/	< -20	/	2023
[26]	39×18	3.1–12	2	2	< -20	< 0.18	2024
[27]	50×100	2–12	2	2	< -15	< 0.5	2024
This	60×30	3.08–10.87	3	2	< -20	< 0.0072	/

shown in Figs. 20(a) and (b), the antenna exhibits relatively smooth and nearly omnidirectional spatial radiation characteristics at lower frequencies (3.2 GHz and 4.5 GHz). As shown in Figs. 20(c) and (d), as the operating frequency increases to 6.5 GHz and 8.0 GHz, slight splitting and distortion begin to appear in three-dimensional radiation patterns, which is highly consistent with changes in two-dimensional radiation patterns observed in Fig. 18.

Table 2 compares the proposed antenna with other UWB MIMO antennas featuring notch filtering. Analysis of the antenna's performance demonstrates that it not only provides band-notch filtering but also exhibits high port isolation and low envelope correlation coefficient. The proposed antenna achieves balance among multi-band suppression, broadband performance, and MIMO performance, making it suitable for applications in modern UWB environments.

4. CONCLUSION

This paper proposes and verifies a dual-port UWB MIMO antenna with triple-notch characteristics based on CPW feeding. The advantages and disadvantages of the proposed design scheme compared to the previously reported scheme: (1) Through three EBG structures on the back of the substrate and an inverted U-shaped slot on the feed line, this antenna achieves triple-band notch characteristics in the WiMAX band (3.3–4.31 GHz), WLAN band (4.82–6.32 GHz), and C-band (6.6–7.71 GHz) within the 3.08–10.87 GHz range, achieving mutual coupling coefficient below -20 dB without additional decoupling structures. (2) The antenna measures 60 mm $\times$ 30 mm $\times$ 1.6 mm. Compared to previous designs, this design occupies a relatively large amount of physical space. The diameter and location of the through-hole have a significant impact on the notch filtering effect. This can lead to significant discrepancies between measured and simulated results. The center frequency gains for each notch band were −4.6 dBi, −11 dBi, and −3.5 dBi, with radiation efficiencies of 36%, 11%, and 23%, respectively. The antenna's ECC and DG performance indicators were less than 0.0072 dB and greater than 9.9997 dB, respectively, representing good MIMO performance. Simulation data and measurement results were in good agreement. In summary, this antenna has a wide bandwidth coverage, multi-notch characteristics, and excellent MIMO performance, and can be used in modern UWB communication systems, portable wireless mobile terminals and devices, 5G, and future high-frequency wireless communication.

ACKNOWLEDGEMENT

This work was supported in part by the Natural Science Research Project of Anhui Educational Committee under Grant No. 2025AHGXZK31006, in part by the Research Foundation of Jiangsu Engineering Research Center for Bionics Control Technology and Equipment under No. FSKZ202503, in part by the Anhui International Joint Research Center for Ancient Architecture Intelligence and Multi-Dimensional Modeling under No. GJZZX2025KF01, and GJZZX2025KF03.

REFERENCES

[1] Jayant, S., G. Srivastava, and S. Kumar, "Quad-port UWB MIMO footwear antenna for wearable applications," *IEEE Transactions on Antennas and Propagation*, Vol. 70, No. 9, 7905–7913, 2022.

[2] Tu, R., H. Lin, and Z. Wang, "A MIMO ultra-wideband antenna with high isolation and triple notches," *Progress In Electromagnetics Research C*, Vol. 159, 91–102, 2025.

[3] Xu, L.-J., J. Zhang, Z. Duan, F. Huang, and Y. Li, "Directly connected linear antenna array with band-notch characteristics for UWB applications," *IEEE Antennas and Wireless Propagation Letters*, Vol. 22, No. 11, 2685–2689, 2023.

[4] Kim, B. and J. Oh, "Dual-wideband low-profile three-notch patch antenna with indirect differential feeding for 5G millimeter-wave applications," *IEEE Antennas and Wireless Propagation Letters*, Vol. 24, No. 9, 2734–2738, 2025.

[5] Wong, K.-L., C.-Y. Wu, W.-T. Li, and W.-Y. Li, "Hybrid MIMO antennas comprising ultra-wideband frame conjoined two-antenna elements in 3.3-8.4 GHz and low-profile backcover four-antenna module in 6.425-8.4 GHz for 5G/6G smartphones," *IEEE Access*, Vol. 13, 91 611–91 624, 2025.

[6] Zhao, Z., C. Zhang, Z. Lu, H. Chu, S. Chen, M. Liu, and G. Li, "A miniaturized wearable antenna with five band-notched characteristics for medical applications," *IEEE Antennas and Wireless Propagation Letters*, Vol. 22, No. 6, 1246–1250, 2023.

[7] Li, J., Y. Yin, M. Yang, S. Li, and H. Zhao, "Analysis and design of multiple narrow reflectionless notched bands integrated UWB monopole antenna," *IEEE Transactions on Antennas and Propagation*, Vol. 73, No. 9, 7027–7032, 2025.

[8] Rekha, V. S. D., P. Pardhasaradhi, B. T. P. Madhav, and Y. U. Devi, "Dual band notched orthogonal 4-element MIMO antenna with isolation for UWB applications," *IEEE Access*, Vol. 8, 145 871–145 880, 2020.

[9] Liu, L., S. W. Cheung, and T. I. Yuk, "Compact MIMO antenna for portable UWB applications with band-notched characteristic," *IEEE Transactions on Antennas and Propagation*, Vol. 63, No. 5, 1917–1924, 2015.

[10] Chandel, R., A. K. Gautam, and K. Rambabu, "Tapered fed compact UWB MIMO-diversity antenna with dual band-notched characteristics," *IEEE Transactions on Antennas and Propagation*, Vol. 66, No. 4, 1677–1684, 2018.

[11] Zhao, L., Y. Wang, C. Liu, D. Song, C. Hu, C. Li, H. Zhao, and Z. Wang, "Compact circular-shaped MIMO antenna covers UWB bandwidth with four frequently-used band-notched characteristics for multi-scenario applications," *IEEE Access*, Vol. 12, 32 762–32 771, 2024.

[12] Shehata, M., M. S. Said, and H. Mostafa, "Dual notched band quad-element MIMO antenna with multitone interference suppression for IR-UWB wireless applications," *IEEE Transactions on Antennas and Propagation*, Vol. 66, No. 11, 5737–5746, 2018.

[13] Tao, J. and Q. Feng, "Compact ultrawideband MIMO antenna with half-slot structure," *IEEE Antennas and Wireless Propagation Letters*, Vol. 16, 792–795, 2017.

[14] Shailesh, , G. Srivastava, M. Al-Hamami, S. Kumar, M. P. Sunil, and O. P. Kumar, "Triple-band notched and highly decoupled MIMO antenna using characteristic mode analysis," *IEEE Access*, Vol. 13, 165 956–165 969, 2025.

[15] Kumar, A., D. Chaturvedi, and F. Sarrazin, "Characterization and modeling of self-diplexing MIMO antenna for endoscopy capsule applications," *International Journal of Communication Systems*, Vol. 38, No. 12, e70179, 2025.

[16] Saraswat, R. K. and M. Kumar, "A metamaterial hepta-band antenna for wireless applications with specific absorption rate reduction," *International Journal of RF and Microwave Computer-Aided Engineering*, Vol. 29, No. 10, e21824, 2019.

[17] Saraswat, R. K., "A hybrid fractal metamaterial inspired multi-band antenna for wireless applications," *Wireless Personal Communications*, Vol. 124, No. 3, 2593–2612, 2022.

[18] Mallani, H., A. Agrawal, and R. K. Saraswat, "Implementation of fractal metamaterial inspired antenna for multi-standard wireless applications," *Progress In Electromagnetics Research B*, Vol. 108, 121–137, 2024.

[19] Suyan, N. K., M. Kumar, and R. K. Saraswat, "Design and analysis of dual band wearable antenna for body centric wireless communication," *IETE Journal of Research*, Vol. 71, No. 9, 3129–3138, 2025.

[20] Saraswat, R. K. and M. Kumar, "A vertex-fed hexa-band frequency reconfigurable antenna for wireless applications," *International Journal of RF and Microwave Computer-Aided Engineering*, Vol. 29, No. 10, e21893, 2019.

[21] Khan, M. I. and M. I. Khattak, "Designing and analyzing a modern MIMO-UWB antenna with a novel stub for stop band characteristics and reduced mutual coupling," *Microwave and Optical Technology Letters*, Vol. 62, No. 10, 3209–3214, 2020.

[22] Yuan, H., F.-S. Zhang, J.-J. Zhang, Y.-X. Feng, and Y.-F. Liu, "A compact ultra-wideband multiple-input-multiple-output antenna with dual band-notched performance using slot-line transmission," *International Journal of RF and Microwave Computer-Aided Engineering*, Vol. 32, No. 5, e23098, 2022.

[23] Kumar, P., T. Ali, and M. P. Mm, "Characteristic mode analysis-based compact dual band-notched UWB MIMO antenna loaded with neutralization line," *Micromachines*, Vol. 13, No. 10, 1599, 2022.

[24] Jayant, S. and G. Srivastava, "Close-packed quad-element triple-band-notched UWB MIMO antenna with upgrading capability," *IEEE Transactions on Antennas and Propagation*, Vol. 71, No. 1, 353–360, 2023.

[25] Chaturvedi, D., A. Kumar, A. A. Althuwayb, and F. Ahmadfard, "SIW-backed multiplexing slot antenna for multiple wireless system integration," *Electronics Letters*, Vol. 59, No. 11, e12826, 2023.

[26] Banerjee, J., A. Gorai, and R. Ghatak, "Development and investigation of a compact band-notched MIMO antenna attaining wideband isolation for UWB applications," *Journal of Electromagnetic Waves and Applications*, Vol. 38, No. 11, 1283–1299, 2024.

[27] Ray, S., I. Ghosh, M. Maity, B. D. Biswas, K. Banerjee, S. Chakraborty, and C. Sarkar, "Circular shaped meta-surface embedded monopole antenna for ultra-wideband MIMO applications with frequency notched characteristics," in *2024 IEEE International Conference on Communication, Computing and Signal Processing (IICCCS)*, 1–4, ASANSOL, India, 2024.